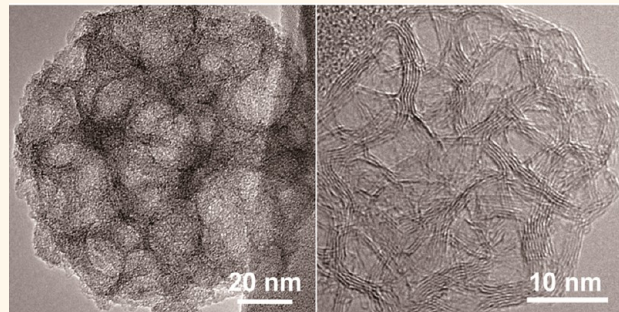


Solution-Based Carbohydrate Synthesis of Individual Solid, Hollow, and Porous Carbon Nanospheres Using Spray Pyrolysis

Chengwei Wang,[†] Yuan Wang,[†] Jake Graser,[†] Ran Zhao,[‡] Fei Gao,[†] and Michael J. O'Connell^{†,*}

[†]Materials Science and Engineering, School for Engineering of Matter, Transport and Energy, and [‡]Department of Chemistry and Biochemistry, Arizona State University, Tempe, Arizona 85287, United States

ABSTRACT A facile and scalable solution-based, spray pyrolysis synthesis technique was used to synthesize individual carbon nanospheres with specific surface area (SSA) up to 1106 m²/g using a novel metal-salt catalyzed reaction. The carbon nanosphere diameters were tunable from 10 nm to several micrometers by varying the precursor concentrations. Solid, hollow, and porous carbon nanospheres were achieved by simply varying the ratio of catalyst and carbon source without using any templates. These hollow carbon nanospheres showed adsorption of up to 300 mg of dye per gram of carbon, which is more than 15 times higher than that observed for conventional carbon black particles. When evaluated as supercapacitor electrode materials, specific capacitances of up to 112 F/g at a current density of 0.1 A/g were observed, with no capacitance loss after 20 000 cycles.



KEYWORDS: carbon nanospheres · mesoporous · high surface area · sorption · supercapacitors

The high surface area of carbon nanostructures such as carbon nanotubes and graphene have made them attractive for a variety of applications such as electrode materials in supercapacitors,^{1–5} fuel cell,^{6,7} batteries,^{8,9} and solar-energy conversion,¹⁰ catalyst supports,¹¹ sensors^{12,13} and adsorbents.^{14,15} For example, single-walled carbon nanotube and single-layer graphene have theoretical surface areas of 1315¹⁶ and 2630 m²/g, respectively. However, in many cases, the effective surface area is much smaller once the carbon nanostructures are deposited onto an electrode because of agglomeration, roping (in the case of nanotubes), or stacking (in the case of graphene). Currently, it is still difficult and expensive to synthesize carbon nanotubes and graphene at large scales.¹⁷ Hence, there is still a need for development of low-cost and facile synthesis techniques for carbon nanostructures with highly accessible surface areas.

For this reason, there has been considerable interest in the synthesis of carbon nanospheres, which are carbon nanoparticles that can be designed with mesoporous or hollow morphologies.^{14,18–21} Compared to nanotubes and graphene, there are a multitude of different methods for synthesizing carbon nanospheres such as laser ablation,²² high temperature transformation of nanodiamond,^{23,24} arc-discharge in water,²⁵ combustion synthesis,²⁶ hydrothermal reaction^{27,28} and separation from soot.²⁹ Mesoporous and hollow carbon nanospheres are often synthesized by using templates such as silica^{18–20} or polymer nanospheres.^{14,21,27,30} Some template-free methods typically result in hollow structures that are interconnected with each other,³¹ which is not good for bioapplication, like drug delivery. Carbon nanospheres have been widely used for lithium-ion battery electrode materials,^{31,32} supercapacitors,^{23,33,34} oil removal,¹⁴ catalyst supports,^{35,36} and biorelated applications.³⁷ Many of the aforementioned

* Address correspondence to moconnell@asu.edu.

Received for review September 17, 2013 and accepted November 25, 2013.

Published online November 25, 2013
10.1021/nn4048759

© 2013 American Chemical Society

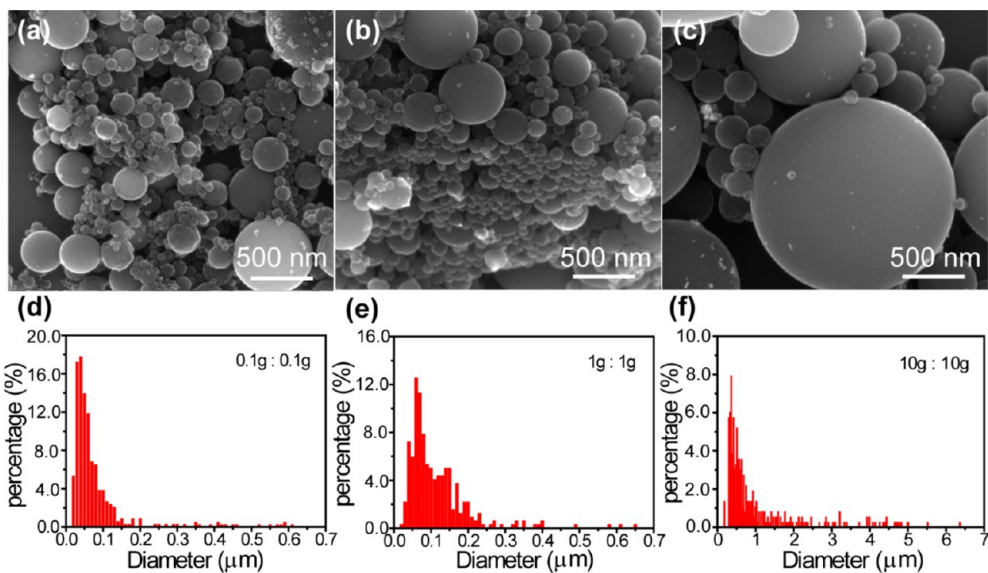


Figure 1. SEM image and size distribution of carbon nanospheres synthesized using spray pyrolysis from different ratios of $(\text{Zn}(\text{NO}_3)_2$ to sugar in 100 mL of DI water. (a,d) 0.1:0.1 g; (b,e) 1:1 g; (c,f) 10:10 g.

methods for synthesizing carbon nanospheres still suffer from low product yields, which can limit their use in these applications.

Spray pyrolysis has been used for the continuous synthesis of many different types of inorganic nanoparticles^{38–40} and can be easily scaled. Spray pyrolysis has been recently applied to the synthesis of carbon nanomaterials. Sohn *et al.*¹⁴ used spray pyrolysis to synthesize graphene capsules, but the method still required the use of polystyrene nanosphere templates. The direct pyrolysis of hydrocarbons⁴¹ has been used to demonstrate the large scale synthesis of carbon spheres. However, this method requires vapor phase or pre-evaporated hydrocarbon solvents and did not demonstrate good particle size control.

Here we report a solution-based, spray pyrolysis synthesis technique able to create individual carbon nanospheres with a high yield and controllable size from precursors consisting of organic carbon precursors and metal salts. The carbon nanosphere diameter distribution was changed by varying the concentration of the precursors. The method also enables the ability to make hollow carbon nanospheres directly without the use of templates by simply adjusting the ratio of precursors. Furthermore, this technique also allows for heteroatom doping of the carbon nanospheres by adding different precursors to the solution. Different metal salts were tested to show the generality for this method and were found to alter the carbon nanosphere structure. Different annealing processes were used to control the structure, and specific surface areas (SSA) up to 1106 m^2/g were demonstrated in hollow carbon nanospheres. Rhodamine blue dye sorption and electrochemical tests showed that these high surface area carbon nanospheres could be used as materials with high sorption capacity and supercapacitors.

RESULTS AND DISCUSSION

Typical scanning electron microscopy (SEM) images of carbon nanospheres synthesized from three different concentrations of sugar and $\text{Zn}(\text{NO}_3)_2$ precursors are shown in Figure 1a–c. In each case, the sugar to $\text{Zn}(\text{NO}_3)_2$ weight ratio was maintained at 1:1, corresponding to 0.1, 1, and 10 g each of sugar and $\text{Zn}(\text{NO}_3)_2$ in 100 mL of DI water, respectively. All of the samples showed a wide particle size distribution. However, as the concentration of precursors increased, the size distribution was shifted toward larger particle sizes, as shown in the histograms in Figure 1d–f. In the 0.1:0.1 g case, most of the particle sizes were smaller than 100 nm. When the precursor ratio was changed from 1:1 g, the median particle size shifted from ~ 30 to ~ 70 nm, while the largest particle size was still below 1 μm . When the precursor ratio was further increased to 10:10 g, the median particle size increased to ~ 300 nm, and the largest particle diameter was more than 5 μm . These results show that the carbon nanosphere size distribution can be adjusted by changing the concentration of reagent precursors.

X-ray diffraction (XRD) measurements were performed on carbon nanospheres prepared using a precursor ratio of 1:1 g. As shown in Figure 2a, the as-prepared sample only showed a few reflections, which matched to ZnO (PDF 01-079-0208 in the ICDD database). This suggests that the as-prepared carbon nanospheres have an amorphous carbon structure and that the $\text{Zn}(\text{NO}_3)_2$ transformed to ZnO during the spray pyrolysis. The XRD pattern after HCl etching showed that the ZnO peaks were no longer visible, suggesting that the ZnO was dissolved during the treatment. Annealing the as-made carbon nanospheres in the tube furnace at 1200 °C for 1 h under Ar (flowing at 100 sccm) resulted in a featureless XRD pattern, indicating that the

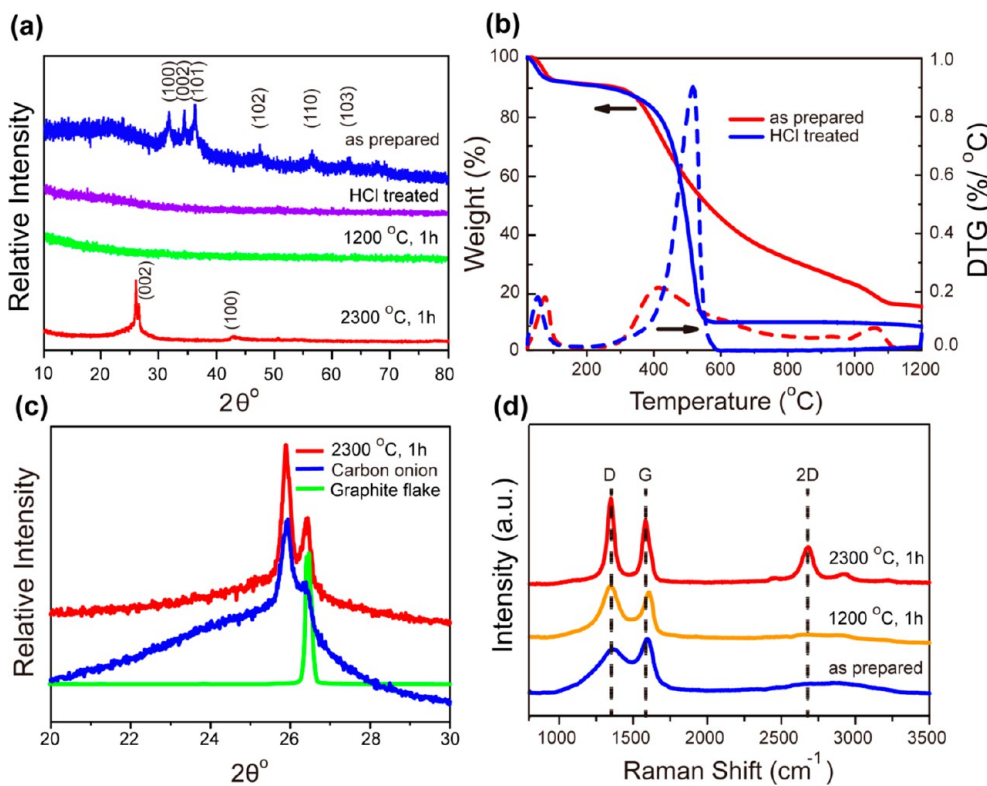


Figure 2. Characterization of carbon nanospheres from 1:1 g precursors. (a) XRD results of products as-prepared (blue), after HCl treatment (purple), after annealing as-prepared products at 1200 °C for 1 h (green), after annealing as-prepared products at 2300 °C for 1 h (red). (b) TGA results for as-prepared carbon nanospheres (red) and after HCl treatment (blue). (c) Zoomed-in XRD pattern around the *d*-spacing for (002) plane of graphite of carbon nanosphere products annealed at 2300 °C for 1 h (red) compared to carbon onions prepared from nanodiamond annealed at same condition (blue) and graphite flake (green). (d) Raman spectra using 532 nm excitation of carbon nanospheres as prepared (blue) and after annealing at 1200 °C (orange) and 2300 °C (red) for 1 h.

carbon remained amorphous. The ZnO peaks were absent as well. Since it is known that ZnO can be reduced by carbon at high temperatures,⁴² it is possible that the ZnO nanoparticles were reduced to Zn and then evaporated, since the boiling point of Zn is only 907 °C.

To better understand these results, thermogravimetric analysis (TGA) (Figure 2b) was performed on the as-prepared 1:1 g carbon nanospheres (which still contained ZnO nanoparticles) and samples after HCl etching (ZnO removed). The initial weight loss for both samples below 200 °C was due to desorption of water and air. The carbon nanosphere sample treated with HCl lost the most weight between 400 and 600 °C, likely because of further carbonization of the remaining organics. For the as-prepared sample, however, the weight kept decreasing even at 1200 °C, while the derivative thermogravimetric (DTG) curve showed another weight loss peak at ~1050 °C, likely due to the evaporation of zinc. Gravimetric measurements performed after annealing ~100 mg of carbon nanosphere sample showed a ~20 wt % weight loss after annealing at 700 °C for 30 min, attributed to the carbonization reactions. After treating the sample with HCl and drying, ~30% of the mass was further lost. This was attributed to the removal of ZnO. Therefore, about 50–60% of the original mass remained as pure carbon.

After annealing the as-made samples at 2300 °C for 1 h, the amorphous carbon nanospheres changed to graphitic structures. This structure change was reflected in the XRD pattern (Figure 2a,c) and confirmed using Raman spectroscopy (Figure 2d). In the XRD pattern, the peak at $2\theta = 43^\circ$ was indexed to the (100) plane for graphite (PDF 00-041-1487). Two peaks were observed very close together at $2\theta = 25.88^\circ$ and 26.45° , with the latter being close to the reflection for the (002) plane of graphite (Figure 2c). This two-peak phenomenon was observed in other literature⁴³ before but without clear explanation. A peak with the former spacing and a broad shoulder near the (002) plane was observed in carbon onions derived from high temperature annealed nanodiamond.⁴⁴ We reproduced this synthesis, and the XRD pattern corresponding to these carbon onions is shown in Figure 2c as comparison. When the XRD pattern of the carbon nanosphere sample annealed at 2300 °C is overlaid with that for nanodiamond-derived carbon onion, as well as pure natural graphite flake, the relationship of these peaks can be clearly observed. Hence the peak at $2\theta = 25.88^\circ$ likely corresponds to the high curvature graphitic faces similar to those found in carbon onions, while the peak at $2\theta = 26.45^\circ$ may come from the low curvature graphitic faces found in graphite. The reason that the

(002) peak splits into two peaks in our carbon nanospheres might correspond to different types of nanoscale curvature inside the nanospheres. This was confirmed with high resolution transmission electron microscopy (TEM) on the carbon onions (Figure S1a, Supporting Information) and carbon nanospheres (Figure S1b, Supporting Information).

The Raman spectra of the carbon nanospheres with different heat treatments are shown in Figure 2d. The D band at $\sim 1360\text{ cm}^{-1}$ is attributed to defect and disorder-induced modes of disordered or glassy carbon.⁴⁵ The peak at $\sim 1590\text{ cm}^{-1}$ is indexed to the G band corresponding to the phonon mode with E_{2g} symmetry of graphite.⁴⁶ Other than the sample annealed at $2300\text{ }^{\circ}\text{C}$ for 1 h, none of the samples have the 2D band at $\sim 2680\text{ cm}^{-1}$, while D and G bands were broad and weak, indicating the presence of significant amounts of disordered carbon. For the sample treated at $2300\text{ }^{\circ}\text{C}$, the ratio of the intensities of the 2D and G bands (I_{2D}/I_G) was equal to 0.57, which reflects a multi-layer graphene structure. This is consistent with the XRD (Figure 2c) and TEM results (Figure S1b, Supporting Information) showing graphitization of the carbon nanospheres after annealing at $2300\text{ }^{\circ}\text{C}$.

In order to study the role of the $\text{Zn}(\text{NO}_3)_2$ during the formation of the carbon nanospheres, the weight ratio of $\text{Zn}(\text{NO}_3)_2$ to sugar was varied. In all cases 1 g sugar and 100 mL of DI water were used. Figure S2 (Supporting Information) shows some typical TEM images of different as-prepared carbon nanospheres using different amounts of $\text{Zn}(\text{NO}_3)_2$. Figure 3 shows the high-magnification TEM images of individual carbon nanospheres prepared using precursor ratios of 1:1 g, 3:1 g, and 10:1 g. Figure 3a shows the high-magnification TEM image of as-prepared carbon nanospheres using 1:1 g. The particles $< 10\text{ nm}$ in diameter on the carbon nanosphere surface correspond to ZnO . As shown in the high resolution TEM image in Figure S2b (Supporting Information), the ZnO nanoparticles were crystalline, with the measured *d*-spacing of 0.28 nm matching the ZnO (100) plane, while the carbon was amorphous, consistent with the XRD results. Figure 3b shows a high magnification TEM image of carbon nanospheres prepared from a precursor solution with 3 g of $\text{Zn}(\text{NO}_3)_2$ to 1 g of sugar (3:1 g). Most of the carbon nanospheres appeared to be covered with larger particles about 20 nm in diameter. When the $\text{Zn}(\text{NO}_3)_2$ to sugar ratio was increased to 10:1 g, the nanoparticles on the surface of the carbon nanospheres also had large diameters greater than 50 nm (Figure 3c). No carbon nanospheres were made when performing spray pyrolysis of sugar solutions without $\text{Zn}(\text{NO}_3)_2$, indicating that the ZnO nanoparticles may play an important role as nucleation sites for the carbonization reactions and promote formation of the carbon nanospheres.

TEM images of carbon nanospheres after HCl treatment are shown in Figure 4 for the different $\text{Zn}(\text{NO}_3)_2$:sugar ratios. The nanoparticles observed in the as-prepared samples were absent after HCl etching,

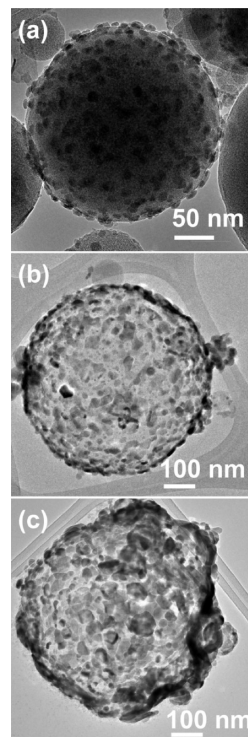


Figure 3. TEM images of carbon nanospheres from $\text{Zn}(\text{NO}_3)_2$ to sugar ratios of (a) 1:1 g; (b) 3:1 g; (c) 10:1 g.

confirming that they were composed of ZnO (Figure 4a,b). In contrast, the as-prepared samples annealed at $2300\text{ }^{\circ}\text{C}$ showed a graphitic structure, consistent with the XRD and Raman results (Figure 2). The ZnO nanoparticles were also absent, confirming the proposed evaporation at the higher annealing temperature, as suggested by the TGA data (Figure 2b). As Figure 4a,b shows, the 1:1 g dots are mostly solid. The 3:1 g products after HCl etching (Figure 4d) consisted of some smaller, solid amorphous carbon nanospheres (Figure 4e), while others appeared to be hollow, "balloon"-like nanospheres with highly porous structures (Figure 4f). After HCl treatment of the samples prepared from the 10:1 g precursor solutions, the resulting carbon nanospheres were highly porous (Figure 4g), and large carbon particles with "balloon" morphology dominated the product (Figure 4i). The smaller carbon nanospheres were also observed to have a highly porous structure (Figure 4h).

No carbon nanospheres were formed when using direct pyrolysis of pure sugar aqueous solutions at the same condition, indicating that ZnO nanoparticles formed during heating of $\text{Zn}(\text{NO}_3)_2$ at high temperature may act as nucleation sites for carbonization of sugar to form carbon nanospheres. From the observed carbon nanosphere morphology dependence on the $\text{Zn}(\text{NO}_3)_2$ concentration used, the formation mechanism for the carbon nanospheres is proposed as follows. When high concentrations of $\text{Zn}(\text{NO}_3)_2$ were used, enough $\text{Zn}(\text{NO}_3)_2$ could accumulate at the surface of

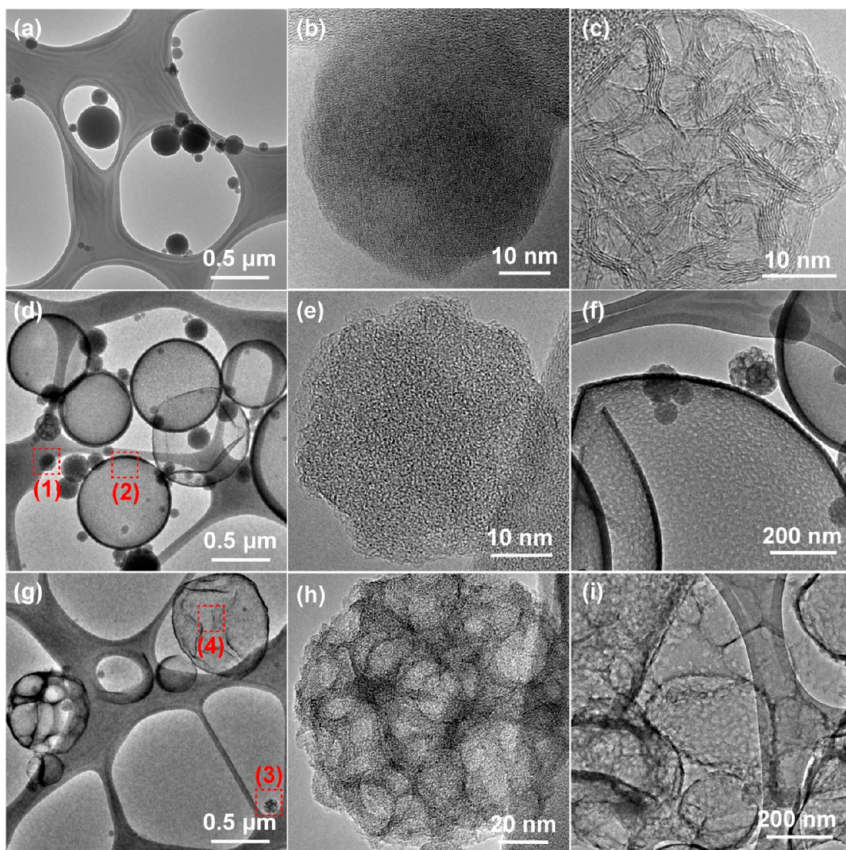


Figure 4. TEM images of carbon nanospheres from different $\text{Zn}(\text{NO}_3)_2$ to sugar ratios after HCl etching. Panels (a–c) were prepared using 1:1 g, (a) and (b) are after HCl etching, whereas (c) shows the as-prepared product after annealing at $2300\text{ }^\circ\text{C}$. Panels (d–f) are prepared using 3:1 g. Panels (e) and (f) show the zoomed in images of particles (1) and (2) in (d), respectively. Panels (g–i) were prepared using 10:1 g. Panels (h) and (i) show the zoomed in images of particles (3) and (4), respectively.

the droplet to reach the critical concentration for which ZnO nanoparticles could nucleate. These ZnO nanoparticles could prevent the formation of solid carbon nanospheres, leaving porous and hollow structures after removal of the ZnO . For precursors with lower concentrations of $\text{Zn}(\text{NO}_3)_2$, there are fewer ZnO nanoparticles, and the precursors can form solid structures after carbonization. This is shown schematically in Figure S3 (Supporting Information). The solid vs hollow nanosphere morphology can also result from differences in the solvent evaporation and solute diffusion times in the precursors, wherein similar time scales for these processes typically result in solid particles, and cases with slow solute diffusion within the droplets result in hollow or crushed particles.⁴⁰

To better understand the growth mechanism of the carbon nanospheres, different metal salts and carbon precursors were also investigated. The carbon nanospheres synthesized using $\text{Zn}(\text{NO}_3)_2$ and 3,4-dihydroxybenzaldehyde (1:1 g) and treated with HCl are shown in Figure S4a (Supporting Information) and showed similar morphologies as those prepared using sugar. Figure S4b,c (Supporting Information) shows the SEM images of carbon nanospheres prepared using sugar as the carbon source and manganese(II) nitrate hydrate

and ferric chloride, respectively, in place of $\text{Zn}(\text{NO}_3)_2$. Using the manganese salt resulted in carbon nanospheres with a rough surface (Figure S4b, Supporting Information). The carbon nanospheres prepared with ferric chloride showed large holes on their surfaces after HCl etching (Figure S4c, Supporting Information). XRD of the as-prepared samples showed that the materials were amorphous, suggesting crystalline iron or manganese oxides did not form during the pyrolysis but that they may be amorphous oxides (Figure S4d, Supporting Information). The broad reflections observed in the sample prepared with the manganese salt are likely from the carbon, since they did not match reflections for MnO_2 . Carbon nanospheres were also synthesized using $\text{Zn}(\text{NO}_3)_2$ and polyethylenimine (PEI) (1:1 g). When PEI was used as the carbon source, the carbon nanospheres showed a deflated shape (Figure S5a, Supporting Information). The ability to use PEI as the carbon source provides the opportunity for preparing nitrogen doped carbon nanospheres. Thiourea was also added to the precursor solution along with the PEI. Figure S5b (Supporting Information) shows the X-ray photoelectron spectroscopy (XPS) wide scan result for as-prepared carbon nanospheres synthesized from 2 g of $\text{Zn}(\text{NO}_3)_2$, 1 g of PEI and 1 g of thiourea.

The peaks from N 1s and S 2p showed that these species were incorporated into the carbon nanospheres from the PEI and thiourea, respectively. The composition determined from XPS was about 55% at C, 12% at N, 19% at S, with the balance being ZnO. These results show that different carbon sources and salts can be used to make the carbon nanospheres, but more studies are required to fully understand their formation mechanism compared to the $Zn(NO_3)_2$ /sugar case.

N_2 adsorption isotherms were used to determine the specific surface area (SSA) of the carbon nanospheres using the Brunauer–Emmett–Teller (BET) method at 77 K. The adsorption isotherms were used to calculate the pore size distribution *via* the Barrett–Joyner–Halenda (BJH) method. Higher precursor concentrations of $Zn(NO_3)_2$ to sugar were used to increase the product yield. Figure S6 (Supporting Information) shows the SEM images of samples prepared from 3:3 g and 6:3 g in 100 mL of water. Although the diameters of the carbon nanospheres became larger, the carbon nanosphere structures were similar to those observed in 1:1 g and 3:1 g samples described above, with the 3:3 g sample displaying predominately solid carbon nanospheres and the 6:3 g sample displaying many porous hollow carbon nanospheres. Figure 5a shows the N_2 adsorption/desorption isotherms, and Table 1 shows the SSA and total pore volumes for carbon nanospheres prepared with different precursor concentrations and subsequent heat treatments. For the sample prepared from 3:3 g followed by treatment with HCl and annealing at 1000 °C for 1 h, the isotherm is classified as type I, which indicates that a microporous structure is generated from the holes when the ZnO nanoparticles were removed with HCl. The SSA of this sample was 920 m^2/g . For the sample prepared from 6:3 g and treated with the same condition, the SSA was almost the same at 928 m^2/g . After annealing both of these samples at 2300 °C for 1 h, the SSAs dropped dramatically to 14 and 42 m^2/g , respectively, indicating disappearance of the microporous structure during the crystallization at high temperature. When these two samples were annealed at 1100 °C directly without removing the ZnO with HCl, the SSA were 1106 and 1036 m^2/g , respectively. This higher SSA compared to the samples with ZnO removed using HCl etching indicates that the ZnO may be etching additional carbon during the high temperature annealing, making the pores bigger. The BET curves from samples prepared with higher $Zn(NO_3)_2$ concentration have larger slopes than samples from low $Zn(NO_3)_2$ concentrations. This corresponds with the hollow carbon nanosphere structures observed in the SEM (Figure S6b, Supporting Information). Importantly, these SSAs are about double those obtained for mesoporous carbon nanospheres synthesized using chemical vapor deposition on polystyrene templates.³⁰ Although the total pore volume may be different for different samples, most of the pore sizes

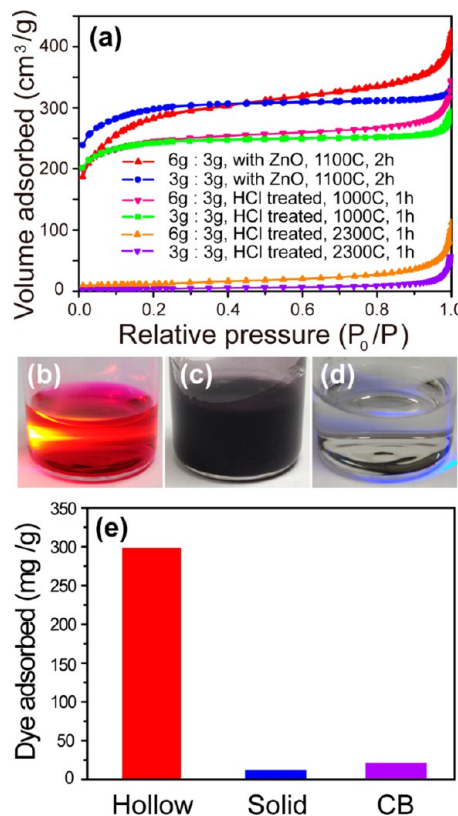


Figure 5. (a) N_2 adsorption–desorption isotherms of different carbon nanospheres. Photographs of (b) 100 mg/L of RB solution under excitation with 405 nm laser, (c) carbon nanospheres suspended in the RB solution, (d) RB solution after carbon nanospheres removed solution with excitation by 405 nm laser. (e) RB adsorption abilities of different samples (mg of dye adsorbed per g of carbon): hollow carbon nanospheres (prepared from 6:3 g followed by annealing at 1100 °C), solid carbon nanospheres (prepared from 3:3 g), and commercial carbon black (CB).

were distributed around 2 nm (Figure S7, Supporting Information).

To make use of the high surface area of the carbon nanospheres, dye adsorption experiments were conducted. The hollow carbon nanospheres prepared from solutions containing 6:3 g $Zn(NO_3)_2$:sugar, followed by annealing at 1100 °C for 2 h (without removing ZnO) were added to a 100 mg/L of rhodamine B (RB) solution (Figure 5b) and suspended with sonication for about 5 min (Figure 5c). After removing the carbon nanospheres with filtration, the clear water could be observed (Figure 5d). UV–vis spectroscopy was used to determine the concentration of the dye remaining in the solution using Beer's law. As shown in Figure S8 (Supporting Information), the remaining RB in solution was only around 0.087 mg/L when 300 mg of dye was mixed with 1 g of carbon nanospheres (300 mg/g). For the solid carbon nanospheres prepared from 3:3 g and treated with same conditions, the dye adsorption ability was much less compared to the hollow materials despite its slightly higher SSA (Table 1). Even when a dye:carbon ratio of only 12 mg/g was used, the concentration

TABLE 1. Specific Surface Area and Pore Volume of Carbon Nanospheres Measured from BET

Zn(NO ₃) ₂ to sugar ratio in precursor	postsynthesis treatment	SSA (m ² /g)	pore volume (cm ³ /g)
3:3 g	HCl etching then heat at 1000 °C for 1 h	920	0.30
6:3 g	HCl etching then heat at 1000 °C for 1 h	928	0.28
3:3 g	HCl treated then heat at 2300 °C for 1 h	14	0.06
6:3 g	HCl treated then heat at 2300 °C for 1 h	42	0.13
3:3 g	heat at 1100 °C for 2 h	1106	0.32
6:3 g	heat at 1100 °C for 2 h	1036	0.40

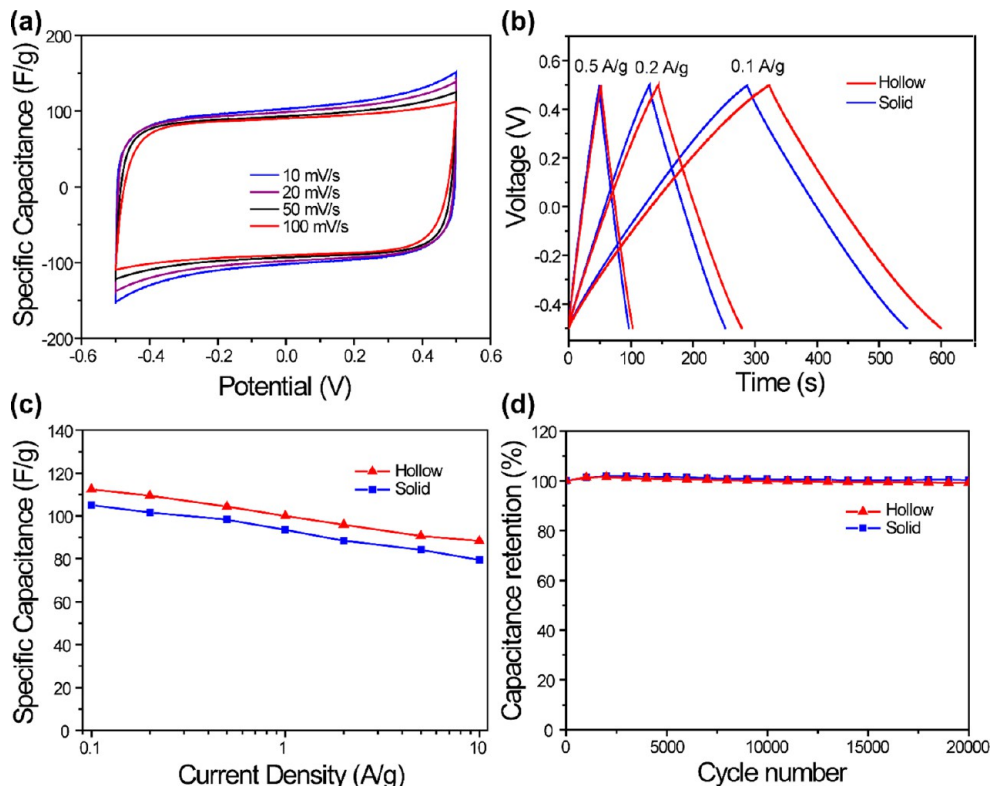


Figure 6. Performance of carbon nanosphere supercapacitors in 6 M KOH aqueous electrolyte. (a) CVs curves obtained using different scan rates for supercapacitor made from hollow carbon nanospheres. **(b)** Galvanostatic charge–discharge curves of supercapacitors made from hollow or solid carbon nanospheres at different current densities. **(c)** The specific capacitance at different current densities. **(d)** Cycle life of different capacitors at a current density of 10 A/g.

of RB that remained in the solution was still as high \sim 1.5 mg/L (Figure S8, Supporting Information). As a comparison, commercially available carbon black with SSA 45 m²/g was found to adsorb \sim 20 mg/g, even higher than the solid carbon nanospheres. The results reveal that for solid carbon nanospheres, the dye molecules may not be able to access the pores inside the nanospheres. Instead, only the external surface could be used for adsorption. For hollow carbon nanospheres, the internal pores are more accessible to the dye molecules, which explains why its adsorption ability is much higher.

To evaluate the performance of the carbon nanospheres as supercapacitor electrode materials, a two-electrode configuration⁴⁷ was used in coin cells with 6 M KOH electrolyte. The cyclic voltammetry (CV) curves from -0.5 to 0.5 V for supercapacitors made from hollow and solid carbon nanospheres are shown in Figure 6a and

Figure S9a (Supporting Information), respectively, while the galvanostatic charge–discharge curves obtained at different current densities are shown in Figure 6b and Figure S9b (Supporting Information). From the internal resistance (IR) drop observed in the discharge curves, the equivalent series resistance (ESR) was around 24 and 30 Ω for the hollow and solid carbon nanospheres, respectively, which is a little high and may be due to the small interfacial contact points between the nanospheres. On the basis of charge–discharge curves, the specific capacitances were 112 and 105 F/g for the hollow and solid carbon nanospheres, respectively, at a current density of 0.1 A/g. Even when the current density increased as high as 10 A/g, the specific capacitances still remained 88.5 and 79.5 F/g, respectively. Similar with the dye adsorption result, the hollow nanospheres had better performance than the solid ones. However, since the electrolyte ion is

much smaller than the dye molecule, the difference in performance was not as significant as in dye adsorption. The specific capacitances observed for our carbon nanospheres are higher than typical values observed in carbon nanotube electrodes (50–100 F/g),⁴⁸ but little lower than those observed in other mesoporous carbon nanospheres (~200 F/g)³⁰ and graphene (100–250 F/g).^{1,2,4,49} The specific capacitance in supercapacitors prepared from both solid and hollow carbon nanospheres was stable with very little decrease, with the final capacitance retention of 100.3 and 99.2% after 20 000 cycles for the solid and hollow nanospheres, respectively. In contrast, only 96% capacitance retention was observed after 10 000 cycles for other mesoporous carbon nanosphere supercapacitors.³⁰

CONCLUSIONS

In summary, we have demonstrated a metal-salt catalyzed, solution-based spray pyrolysis synthesis

technique able to create individual carbon nanospheres. The particle size could be easily adjusted from ~10 nm to several micrometers by changing the concentration of the precursors. By adjusting the ratio of carbon to metal-salt precursors, hollow or solid nanospheres could be acquired without requiring templates. The study indicates that many kinds of metal salts can be used to form crystalline or amorphous oxides that act as nucleation sites and catalyze the formation of carbon nanospheres. After the removal of the metal oxides using acid or annealing at high temperature, porous-structure carbon spheres with SSA as high as 1106 m²/g are produced. These materials could be very promising for applications such as drug delivery and supercapacitors. The strong adsorption ability of the carbon nanospheres also makes them very promising as sorbents for water purification and environmental remediation.

METHODS

Synthesis. In a typical experiment, precursor solutions were prepared by dissolving sugar (sucrose, Alfa Aesar) and Zn(NO₃)₂·6H₂O (Alfa Aesar) in 100 mL of deionized (DI) water, which was placed in a 250 mL 3-neck round-bottom flask. The 3-neck flask was attached to a tube furnace through its middle ground glass joint. An airbrush was fitted to the top ground glass joint such that the nozzle was aimed into the flask to create a swirling mist of the aqueous precursor solution. The swirling mist returned larger droplets to the bottom of the flask to be recirculated and injected smaller droplets into the tube furnace. This gave a rough means to control the droplet size. Nitrogen was used as the carrier gas with a flow rate of 5–8 L/min, while the air brush (Crescendo, Model 175) was adjusted to supply the feedstock at 10–15 mL/h into the tube furnace. In order to increase the residence time of the precursors at high temperature, two 1 in tube furnaces (Lindberg, HTF55322C and TF55035A-1) were placed in series with a 120 cm long quartz tube connecting the furnaces. The furnaces were heated to 900 and 1000 °C, respectively. The exit flange was equipped a 6.35 mm stainless steel tube that was placed into a 250 mL beaker filled with DI water to collect the products. The carbon nanospheres were recovered by vacuum filtration (Millipore FSLP, 0.2 μm). Some samples were treated with acid postsynthesis by placing the powders in 1 M HCl and sonicating for 5 min followed by vacuum filtration and washing with DI water. Carbon nanospheres were also synthesized using 3,4-dihydroxybenzaldehyde (Acros), poly(ethyleneimine) (PEI; branched, M_w ~25 000, Sigma-Aldrich), manganese(II) nitrate hydrate (Alfa Aesar), ferric chloride (Spectrum), and thiourea (Sigma-Aldrich) as precursors. High-temperature annealing experiments were performed by heating several tens of milligrams of as-prepared carbon nanospheres at 1000–1200 °C under N₂ gas flowing at 150 sccm for 0.5–2 h. For some samples, a graphite furnace (GT Thermal Technologies, Inc., Model: 1050CG) was used to anneal the samples at 2300 °C for 1 h in Ar.

Materials Characterization. Carbon nanosphere samples were characterized using scanning electron microscopy (SEM, NOVA 200 Nanolab SEM at 10 kV), transmission electron microscopy (TEM, Phillips CM 200 at 200 kV), X-ray diffraction (XRD, PANalytical X'Pert Pro diffractometer with Cu K α radiation), thermal gravimetric analysis (TGA, Setaram TG-DTA92), Brunauer–Emmett–Teller (BET) surface area analysis (Micromeritics, Tristar II), and Raman spectroscopy (532 nm, 50 mW excitation laser), X-ray photoelectron spectroscopy (XPS, VG ESCALAB 220i-XL with Al K α anode). For XRD comparison, pure natural graphite flake (~10 mesh, Alfa Aesar) was used.

Dye Adsorption. UV–vis spectroscopy (StellarNet, BLACK-Comet C-SR-50) was used to determine the concentration of Rhodamine blue (RB, MP biomedicals) in the dye adsorption experiments. A calibration curve in the range of 0 to 2.5 mg/L of RB was prepared. The concentration of RB remaining in the water after sorption experiments was determined with Beer's law by measuring the absorbance of the solution and using an extinction coefficient of 106 000 M⁻¹ cm⁻¹ for RB. The carbon black used for comparison was obtained from Timcal (SUPER C45).

Electrochemical Measurement. A two-electrode set up was used to measure the performance of the supercapacitors by cyclic voltammetry with a BioLogic VMP3 potentiostat from –0.5 to 0.5 V. The carbon nanosphere powder was deposited onto stainless steel discs (1.5 cm diameter) directly to make ~0.5 mg/cm² electrode. Then two identical electrodes were assembled into a coin cell with Whatman filter paper as separator and 6 M KOH as the electrolyte. The coin cell was pressed to seal at around 1200 psi. The specific capacitance was calculated from galvanostatic charge–discharge curves with the following equation:⁴⁷

$$C = 4I/(m\Delta V/\Delta t)$$

where I is the current used, m is the total mass of carbon nanospheres for both electrodes, and $\Delta V/\Delta t$ was calculated from the slope of the straight part of discharge curve.

Conflict of Interest: The authors declare no competing financial interest.

Acknowledgment. The authors gratefully acknowledge the use of facilities within the LeRoy Eyring Center for Solid State Science, the Goldwater Environmental Laboratory at Arizona State University. We would also like to thank C. K. Chan for valuable discussions. We would like to thank D. Wright for assistance with the high temperature annealing measurements and C. Guo for assistance with the Raman measurements. This work was supported by new faculty startup funds from the Fulton Schools of Engineering at Arizona State University.

Supporting Information Available: HRTEM of nanodiamond derived carbon onions and carbon nanospheres annealed at same condition 2300 °C for 1 h, TEM images of as-prepared carbon nanospheres synthesized from different Zn(NO₃)₂ to sugar ratios, illustration of the carbon nanospheres formation mechanism, SEM images and XRD of carbon nanospheres synthesized from different carbon and metal-salt precursors after HCl treatment, SEM image and XPS results of as-prepared carbon nanospheres synthesized from Zn(NO₃)₂ and PEI, SEM

images of carbon nanospheres prepared from precursors with $Zn(NO_3)_2$ to sugar ratios of 3:3 g and 6:3 g, calibration curve used to determine concentration of RB using UV-vis spectroscopy and corresponding concentrations of remaining RB after sorption onto different carbon samples, pore size distribution curves of different carbon nanospheres, CVs curves at different scan rates for capacitor made of solid carbon nanospheres in 6 M KOH aqueous electrolyte, galvanostatic charge/discharge curves of supercapacitors made from hollow or solid carbon nanospheres at different current densities. This material is available free of charge via the Internet at <http://pubs.acs.org>.

REFERENCES AND NOTES

- Zhu, Y.; Murali, S.; Stoller, M. D.; Ganesh, K. J.; Cai, W.; Ferreira, P. J.; Pirkle, A.; Wallace, R. M.; Cybrosz, K. A.; Thommes, M.; et al. Carbon-Based Supercapacitors Produced by Activation of Graphene. *Science* **2011**, *332*, 1537–1541.
- Yoo, J. J.; Balakrishnan, K.; Huang, J.; Meunier, V.; Sumpter, B. G.; Srivastava, A.; Conway, M.; Reddy, A. L. M.; Yu, J.; Vajtai, R.; et al. Ultrathin Planar Graphene Supercapacitors. *Nano Lett.* **2011**, *11*, 1423–1427.
- Lin, J.; Zhang, C.; Yan, Z.; Zhu, Y.; Peng, Z.; Hauge, R. H.; Natelson, D.; Tour, J. M. 3-Dimensional Graphene Carbon Nanotube Carpet-Based Microsupercapacitors with High Electrochemical Performance. *Nano Lett.* **2013**, *13*, 72–78.
- Luo, J.; Jang, H. D.; Huang, J. Effect of Sheet Morphology on the Scalability of Graphene-Based Ultracapacitors. *ACS Nano* **2013**, *7*, 1464–1471.
- Simon, P.; Gogotsi, Y. Materials for Electrochemical Capacitors. *Nat. Mater.* **2008**, *7*, 845–854.
- Wang, C.; Waje, M.; Wang, X.; Tang, J. M.; Haddon, R. C. Proton Exchange Membrane Fuel Cells with Carbon Nanotube Based Electrodes. *Nano Lett.* **2004**, *4*, 345–348.
- Gong, K.; Du, F.; Xia, Z.; Durstock, M.; Dai, L. Nitrogen-Doped Carbon Nanotube Arrays with High Electrocatalytic Activity for Oxygen Reduction. *Science* **2009**, *323*, 760–764.
- Wang, H.; Yang, Y.; Liang, Y.; Robinson, J. T.; Li, Y.; Jackson, A.; Cui, Y.; Dai, H. Graphene-Wrapped Sulfur Particles as a Rechargeable Lithium-Sulfur Battery Cathode Material with High Capacity and Cycling Stability. *Nano Lett.* **2011**, *11*, 2644–2647.
- Hu, L.; Wu, H.; La Mantia, F.; Yang, Y.; Cui, Y. Thin, Flexible Secondary Li-Ion Paper Batteries. *ACS Nano* **2010**, *4*, 5843–5848.
- Kongkanand, A.; Domínguez, R. M.; Kamat, P. V. Single Wall Carbon Nanotube Scaffolds for Photoelectrochemical Solar Cells. Capture and Transport of Photogenerated Electrons. *Nano Lett.* **2007**, *7*, 676–680.
- Ostojic, G. N.; Liang, Y. T.; Hersam, M. C. Catalytically Active Nanocomposites of Electronically Coupled Carbon Nanotubes and Platinum Nanoparticles Formed via Vacuum Filtration. *Nanotechnology* **2009**, *20*, 434019.
- Huang, J.; Ng, A. L.; Piao, Y.; Chen, C.-F.; Green, A. a; Sun, C.-F.; Hersam, M. C.; Lee, C. S.; Wang, Y. Covalently Functionalized Double-Walled Carbon Nanotubes Combine High Sensitivity and Selectivity in the Electrical Detection of Small Molecules. *J. Am. Chem. Soc.* **2013**, *135*, 2306–2312.
- Jariwala, D.; Sangwan, V. K.; Lauhon, L. J.; Marks, T. J.; Hersam, M. C. Carbon Nanomaterials for Electronics, Optoelectronics, Photovoltaics, and Sensing. *Chem. Soc. Rev.* **2013**, *42*, 2824–2860.
- Sohn, K.; Joo, N. Y.; Chang, H.; Roh, K.-M.; Dong Jang, H.; Huang, J. Oil Absorbing Graphene Capsules by Capillary Molding. *Chem. Commun.* **2012**, *48*, 5968–5970.
- Sun, H.; Xu, Z.; Gao, C. Multifunctional, Ultra-flyweight, Synergistically Assembled Carbon Aerogels. *Adv. Mater.* **2013**, *25*, 2554–2560.
- Peigney, A.; Laurent, C.; Flahaut, E.; Bacsa, R. R.; Rousset, A. Specific Surface Area of Carbon Nanotubes and Bundles of Carbon Nanotubes. *Carbon* **2001**, *39*, 507–514.
- Liang, Y. T.; Hersam, M. C. Highly Concentrated Graphene Solutions via Polymer Enhanced Solvent Exfoliation and Iterative Solvent Exchange. *J. Am. Chem. Soc.* **2010**, *132*, 17661–17663.
- Joo, J. B.; Kim, P.; Kim, W.; Kim, J.; Kim, N. D.; Yi, J. Simple Preparation of Hollow Carbon Sphere via Templating Method. *Curr. Appl. Phys.* **2008**, *8*, 814–817.
- Hampsey, J. E.; Hu, Q.; Wu, Z.; Rice, L.; Pang, J.; Lu, Y. Templating Synthesis of Ordered Mesoporous Carbon Particles. *Carbon* **2005**, *43*, 2977–2982.
- Titirici, M.-M.; Thomas, A.; Antonietti, M. Replication and Coating of Silica Templates by Hydrothermal Carbonization. *Adv. Funct. Mater.* **2007**, *17*, 1010–1018.
- Yan, Y.; Zhang, F.; Meng, Y.; Tu, B.; Zhao, D. One-Step Synthesis of Ordered Mesoporous Carbonaceous Spheres by an Aerosol-Assisted Self-Assembly. *Chem. Commun.* **2007**, *1*, 2867–2869.
- Sun, Y.-P.; Zhou, B.; Lin, Y.; Wang, W.; Fernando, K. A. S.; Pathak, P.; Meziani, M. J.; Harruff, B. A.; Wang, X.; Wang, H.; et al. Quantum-Sized Carbon Dots for Bright and Colorful Photoluminescence. *J. Am. Chem. Soc.* **2006**, *128*, 7756–7757.
- Pech, D.; Brunet, M.; Durou, H.; Huang, P.; Mochalin, V.; Gogotsi, Y.; Taberna, P.-L.; Simon, P. Ultrahigh-Power Micrometre-Sized Supercapacitors Based on Onion-Like Carbon. *Nat. Nanotechnol.* **2010**, *5*, 651–654.
- Zou, Q.; Wang, M. Z.; Li, Y. G.; Lu, B. High-Resolution Transmission-Electron Microscope Characterization of Onionlike Carbon Transformed from Nanodiamond. *J. Vac. Sci. Technol., B* **2010**, *28*, 935–939.
- Sano, N.; Wang, H.; Chhowalla, M.; Alexandrou, I.; Amaralunga, G. A. J. Synthesis of Carbon 'Onions' in Water. *Nature* **2001**, *414*, 506–507.
- Choucair, M.; Stride, J. A. The Gram-Scale Synthesis of Carbon Onions. *Carbon* **2012**, *50*, 1109–1115.
- Tang, K.; Fu, L.; White, R. J.; Yu, L.; Titirici, M.-M.; Antonietti, M.; Maier, J. Hollow Carbon Nanospheres with Superior Rate Capability for Sodium-Based Batteries. *Adv. Energy Mater.* **2012**, *2*, 873–877.
- Yao, C.; Shin, Y.; Wang, L.; Windisch, C. F.; Samuels, W. D.; Arey, B. W.; Wang, C.; Risen, W. M.; Exarhos, G. J. Hydrothermal Dehydration of Aqueous Fructose Solutions in a Closed System. *J. Phys. Chem. C* **2007**, *115*, 15141–15145.
- Liu, H.; Ye, T.; Mao, C. Fluorescent Carbon Nanoparticles Derived from Candle Soot. *Angew. Chem., Int. Ed.* **2007**, *46*, 6473–6475.
- Lee, J.-S.; Kim, S.-I.; Yoon, J.-C.; Jang, J.-H. Chemical Vapor Deposition of Mesoporous Graphene Nanoballs for Supercapacitor. *ACS Nano* **2013**, *7*, 6047–6055.
- Han, F.-D.; Bai, Y.-J.; Liu, R.; Yao, B.; Qi, Y.-X.; Lun, N.; Zhang, J.-X. Template-Free Synthesis of Interconnected Hollow Carbon Nanospheres for High-Performance Anode Material in Lithium-Ion Batteries. *Adv. Energy Mater.* **2011**, *1*, 798–801.
- Xia, Y.; Xiao, Z.; Dou, X.; Huang, H.; Lu, X.; Yan, R.; Gan, Y.; Zhu, W.; Tu, J.; Zhang, W.; et al. Green and Facile Fabrication of Hollow Porous MnO/C Microspheres from Microalgae for Lithium-Ion Batteries. *ACS Nano* **2013**, *7*, 7093–7092.
- Wang, Q.; Yan, J.; Wang, Y.; Ning, G.; Fan, Z.; Wei, T.; Cheng, J.; Zhang, M.; Jing, X. Template Synthesis of Hollow Carbon Spheres Anchored on Carbon Nanotubes for High Rate Performance Supercapacitors. *Carbon* **2013**, *52*, 209–218.
- Ma, F.; Zhao, H.; Sun, L.; Li, Q.; Huo, L.; Xia, T.; Gao, S.; Pang, G.; Shi, Z.; Feng, S. A Facile Route for Nitrogen-Doped Hollow Graphitic Carbon Spheres with Superior Performance in Supercapacitors. *J. Mater. Chem.* **2012**, *22*, 13464–13468.
- Sun, S.; Jaouen, F.; Dodelet, J.-P. Controlled Growth of Pt Nanowires on Carbon Nanospheres and Their Enhanced Performance as Electrocatalysts in PEM Fuel Cells. *Adv. Mater.* **2008**, *20*, 3900–3904.
- Su, F.; Tian, Z.; Poh, C. K.; Wang, Z.; Lim, S. H.; Liu, Z.; Lin, J. Pt Nanoparticles Supported on Nitrogen-Doped Porous Carbon Nanospheres as an Electrocatalyst for Fuel Cells. *Chem. Mater.* **2010**, *22*, 832–839.
- Yang, S.-T.; Cao, L.; Luo, P. G.; Lu, F.; Wang, X.; Wang, H.; Meziani, M. J.; Liu, Y.; Qi, G.; Sun, Y.-P. Carbon Dots for Optical Imaging *In Vivo*. *J. Am. Chem. Soc.* **2009**, *131*, 11308–11309.

38. Suh, W. H.; Suslick, K. S. Magnetic and Porous Nanospheres from Ultrasonic Spray Pyrolysis. *J. Am. Chem. Soc.* **2005**, 127, 12007–12010.
39. Bang, J. H.; Helmich, R. J.; Suslick, K. S. Nanostructured ZnS: Ni²⁺ Photocatalysts Prepared by Ultrasonic Spray Pyrolysis. *Adv. Mater.* **2008**, 20, 2599–2603.
40. Okuyama, K.; Wuled Lenggoro, I. Preparation of Nanoparticles via Spray Route. *Chem. Eng. Sci.* **2003**, 58, 537–547.
41. Jin, Y. Z.; Gao, C.; Hsu, W. K.; Zhu, Y.; Huczko, A.; Bystrzejewski, M.; Roe, M.; Lee, C. Y.; Acquah, S.; Kroto, H.; et al. Large-Scale Synthesis and Characterization of Carbon Spheres Prepared by Direct Pyrolysis of Hydrocarbons. *Carbon* **2005**, 43, 1944–1953.
42. Chen, H.-K. Kinetic Study on the Carbothermic Reduction of Zinc Oxide. *Scand. J. Metall.* **2001**, 30, 292–296.
43. Qiu, J.; Li, Y.; Wang, Y.; Liang, C.; Wang, T.; Wang, D. A Novel Form of Carbon Micro-Balls from Coal. *Carbon* **2003**, 41, 767–772.
44. Qian, J.; Pantea, C.; Huang, J.; Zerda, T. W.; Zhao, Y. Graphitization of Diamond Powders of Different Sizes at High Pressure–High Temperature. *Carbon* **2004**, 42, 2691–2697.
45. Jawhari, T.; Barcelona, U. D.; Investigacion, D. Raman Spectroscopic Characterization of Some Commercially Available Carbon Black Materials. *Carbon* **1995**, 33, 1561–1565.
46. Malard, L. M.; Pimenta, M. A.; Dresselhaus, G.; Dresselhaus, M. S. Raman Spectroscopy in Graphene. *Phys. Rep.* **2009**, 473, 51–87.
47. Stoller, M. D.; Ruoff, R. S. Best Practice Methods for Determining an Electrode Material's Performance for Ultracapacitors. *Energy Environ. Sci.* **2010**, 3, 1294–1301.
48. Zhang, L. L.; Zhao, X. S. Carbon-Based Materials as Supercapacitor Electrodes. *Chem. Soc. Rev.* **2009**, 38, 2520–2531.
49. Wang, Y.; Shi, Z.; Huang, Y.; Ma, Y.; Wang, C.; Chen, M.; Chen, Y. Supercapacitor Devices Based on Graphene Materials. *J. Phys. Chem. C* **2009**, 113, 13103–13107.